Sensors and Actuators B 225 (2016) 563–571

Contents lists available at ScienceDirect

Sensors and Actuators B: Chemical

journal homepage: www.elsevier.com/locate/snb

High-throughput single cell multidrug resistance analysis with multifunctional gradients-customizing microfluidic device

Yiwei Li [1], Dongjuan Chen [1], Yifang Zhang, Chao Liu, Peng Chen, Yachao Wang, Xiaojun Feng, Wei Du, Bi-Feng Liu *

Britton Chance Center for Biomedical Photonics at Wuhan National Laboratory for Optoelectronics – Hubei Bioinformatics & Molecular Imaging Key Laboratory, Systems Biology Theme, Department of Biomedical Engineering, College of Life Science and Technology, Huazhong University of Science and Technology, Wuhan, 430074, China

ARTICLE INFO

Article history:
Received 1 August 2015
Received in revised form 21 October 2015
Accepted 22 November 2015
Available online 2 December 2015

Keywords:
Multidrug resistance analysis
Microfluidic chip
Concentration gradient
HepG2

ABSTRACT

Multidrug resistance analysis represents a great challenge in cancer chemotherapy, drug development and pathological study. In this paper, multifunctional gradients-customizing microfluidic devices were developed for high-throughput single-cell multidrug resistance (MDR) analysis. The gradient profile was determined by the lengths of the distribution microchannels regardless of flow rates and pressure, which provided good stability and remarkably reduced redundancy of microfluidic architecture. The drug of gradient concentrations consecutively stimulate upon the cells in the downstreaming cell cultivation chamber. Time-dependent drug efflux kinetics of HepG2 cells were firstly investigated on our device using both the different-single-cell and the same-single-cell strategies. Furthermore, hepatic polarized HepG2 cells, which collected the secreted cholephilic substances in the apical vacuoles, were used as model to investigate the inhibition of MDR-associated protein with secretion inhibitor cyclosporine A of varied concentrations on single organelle level. Finally, a high-throughput drug screening experiment was conducted to examine both the chemo-sensitizing effect and the cytotoxity of the potential chemo-sensitizing agents. Conclusively, the results confirmed that our method was a highly efficient way to analyze multidrug resistance (MDR) at single-cell or even single-organelle level with advantages of high-throughput, flexibility, stability and low sample consumption.

1. Introduction

Multidrug resistance (MDR) is a serious condition that disease-causing organisms such as bacteria, viruses or neoplastic (cancerous) cells exhibit resistance to distinct drugs or chemicals, e.g., antibiotics or chemotherapy drugs [1–3]. The mechanism of MDR is complicated [4]. Many factors, including the increased efflux of drug, enzymatic deactivation, decreased permeability, altered binding-sites and alternate metabolic pathways, contribute to MDR of cancer cells [4–7]. Among these factors, efflux mechanism is a significant contributor for MDR of neoplastic cells [1,8]. Thus, how to block the efflux of drug is crucial in current cancer treatment [9,10]. It has been proved that MDR-associated proteins (e.g., MRP2, a human conjugate export pump that transports anionic conjugates and certain amphiphilic anions across the apical membrane of polarized cells) play a dominant role in the drug efflux [11,12]. These MDR-associated efflux pumps actively transport drugs out of the cancer cell, which reduce the amount of intracellular drug to a concentration lower than the drug's cytotoxic threshold within the cell [4].

Blocking the efflux is an efficient way to improve chemotherapy sensitivity [13]. Combining inhibitors/modulators (such as cyclosporine A, a broad spectrum multidrug resistance modulator) of MDR-associated proteins with chemotherapy has been proved as a novel treatment strategy [14–16]. To explore and investigate MDR modulators or MDR-associated protein inhibitors, plate reader-based and cytometry-based methods are widely used [17–19]. However, for these commonly used techniques, lack of real time dynamic information at single cell resolution and large sample consumption might be the two major drawbacks in MDR analysis.

Recently, microfluidic chips have been well developed for various biological analysis such as cytotoxicity analysis [20,21], DNA damage analysis [22] and pathogen detection [23]. Benefiting from its ability to well define the biochemical microenvironment in both spatial and temporal resolution, cell-based or even tissue-based

* Corresponding author. Tel.: +86 27 87792203; fax: +86 27 87792170.
E-mail address: bfliu@mail.hust.edu.cn (B.-F. Liu).
[1] These authors contributed equally to this work.

http://dx.doi.org/10.1016/j.snb.2015.11.097
0925-4005/

assay on chip have been widely studied for pharmacological analysis and drug screen [24]. More recently, Li's group has combined microfluidic approach with the same-single-cell analysis to investigate the modulation of MDR, manifested as the inhibition of drug efflux [25,26]. A single MDR cancer cell can be selected and retained in a retention structure for MDR investigation. This technique was able to record the dynamic information of drug efflux and reveal heterogeneity of MDR at single cell level. However, the throughput of this same-single-cell analysis chip is limited, arising from individual cell analysis at a time. Here, we develop novel microfluidic devices enabling to analyze MDR in a high-throughput way, which will further benefit drug screening of chemo-sensitizing agents.

To achieve high-throughput MDR analysis, a microfluidic chip with single-step dilution was designed to generate customized dilutions, in which the dilution ratios of two stock solutions were determined by the length of the distribution channels. Three types of dilution chips for forming linear gradient concentrations (0, 1/7, 2/7, 3/7, 4/7, 5/7, 6/7, 1), exponential gradient concentrations (1/32, 1/16, 1/8, 1/4, 1/2, 1), and stepwise linear gradient dilutions (0, 1/25, 2/25, 3/25, 4/25, 1/5, 2/5, 3/5, 4/5, 1) were fabricated. There are several advantages of our system over the widely used diffusion-based chip and the serial dilution chip. Diffusion-based dilution devices were made to generate concentrations in a simple way, but it is difficult to obtain linear concentration gradients due to the intrinsic error function profile of the diffusion mechanism. Furthermore, it was highly affected by the molecular size, flow rate, diffusion length, and the liquid viscosity. In comparison to the diffusion-based chip, our devices are much more stable and reliable [27,28]. Serial dilution device was firstly proposed by Whitesides' group. And then, several modified stepwise concentration gradient devices were developed for improvement or new applications. Basically, the gradients were generated by repeatedly combining and splitting solutions. However, in this kind of dilution microfluidic network, micromixers or long mixing channels were employed to ensure the prefect mixing in each combining/splitting step. The complexity of the structure dramatically increased as the number of the concentration increasing. In comparison with the serial dilution device, the design of our single-step dilution device is much more simple and easily scaled up [29–33]. Both computational fluid dynamics (CFD) simulation and flow visualization experiment were employed to validate our customized dilution microfluidic chips. For MDR analysis, the flows of drug with concentration gradients were used to stimulate cells in the downstreaming cell cultivation chamber. The drug efflux kinetics was firstly analyzed using both the different-single-cell and the same-single-cell strategies. HepG2 (a cancer cell line) cells, which retained hepatic polarity and formed apical vacuoles for the collection of secreted cholephilic substances, were used as a model to investigate the drug efflux upon the concentration gradients of a secretion inhibitor cyclosporine A.[34,35] Furthermore, these devices were successfully used for drug screening by combining chemotherapy (doxorubicin) and a MDR modulator (concentration gradients of cyclosporine A).[36] Conclusively, using our chip, multiple information of MDR at single-cell level or even single-organelle level could be obtained in a high-throughput way, which proved that our method was a highly efficient way to examine MDR with advantages of flexibility, stability and low sample consumption.

2. Materials and methods

2.1. Principle of single-step dilution

On-chip single-step dilution was achieved by the adjustment of volumetric flow rate, which was simply determined by the distribution channels delivering the two stock solutions with negative pressure applied at the outlet of the microfluidic chip. To determine the exact pressure distribution in the distribution channels, a theoretical model was established. Since the microscale flow was laminar in the channels due to the low Reynolds number, the pressure drop could be described by the Hagen–Poiseuille equation,

$$\Delta P = \frac{8\mu L Q}{\pi r^4} \tag{1}$$

where ΔP, μ, L, Q and r represent the pressure drop, the dynamic viscosity of the fluid, the length of the microchannel, the volumetric flow rate and the effective radius of the microchannel, respectively. Supposed that the volumetric flow rate remains constant for the laminar flows, Eq. (1) for two stock solutions can be described as following:

$$Q_a = \frac{\pi(P_{inlet} - P_{confluent})r^4}{8\mu L_a} \tag{2}$$

$$Q_b = \frac{\pi(P_{inlet} - P_{confluent})r^4}{8\mu L_b} \tag{3}$$

where Q_a and Q_b represent the volumetric flow rates of laminar flows of two stock solutions. P_{inlet}, $P_{confluent}$, L_a and L_i represent the pressures on inlet and confluent point, and the lengths of the bifurcated channels for stock solution a and b, respectively. Deriving from Eqs. (2) and (3), we can have:

$$\frac{Q_a}{Q_b} = \frac{L_b}{L_a} \tag{4}$$

Eq. (4) reveals the general mathematical relationship between pressures and channel lengths at distribution channels. The distribution of volumetric flow rates (Q_a/Q_b) is equal to L_b/L_a. The dilution ratio is calculated from the distribution of volumetric flow rates (Q_a/Q_b). Thus, the expected concentration ($C_{expected}$) can be calculated from the ratio of the lengths of bifurcated channels:

$$C_{expected} = \frac{Q_a \times C_a + Q_b \times C_b}{Q_a + Q_b} = \frac{L_a \times C_b + L_b \times C_a}{L_a + L_b} \tag{5}$$

where C_a and C_b represent the concentration of two stock solutions a and b. Eq. (5) could be further validated by both numerical simulations and flow visualization experiments.

2.2. Materials and reagents

Chemicals such as K_2HPO_4, KH_2PO_4, NaOH, NaCl, HCl, KCl, $CaCl_2$, $MgCl_2$, D-glucose, HEPES, and fluorescein were purchased from Sinopharm Chemical Reagent (Shanghai, China). Rabbit-anti-MRP2 and Goat-anti-rabbit/RBITC were purchased from Beijing Biosynthesis Biotechnology Company (Beijing, China). Fluo-3/AM was obtained from Biotium (CA, USA). Dimethyl sulfoxide (DMSO) and cyclosporine A were obtained from Sigma–Aldrich (USA). Tyrode's solution contained NaCl (137 mM), KCl (5.4 mM), $CaCl_2$ (1.3 mM), $MgCl_2$ (1.0 mM), D-glucose (10 mM) and HEPES (10 mM) was used as the buffer solution (pH 7.2), which was filtered through a 0.22 μm porous membrane for sterilization. Fluorescein was prepared in the buffer solution at a final concentration of 20 μM. The stock solution of 2 mM fluo-3/AM in DMSO was diluted by buffer solution at a final concentration of 1.0 μM. Water used for all the solutions preparation was purified by the Direct-Q system (Millipore, Bedford, MA, USA) and filtered with 0.45 μm sterilized syringe filters prior to use.

2.3. Cell culture

HepG2 cells were cultured in culture flasks (BD Falcon) containing 5.0 ml DMEM medium with 10% (v/v) fetal bovine serum, 100 U/ml penicillin and 100 μg/ml streptomycin. All cells were

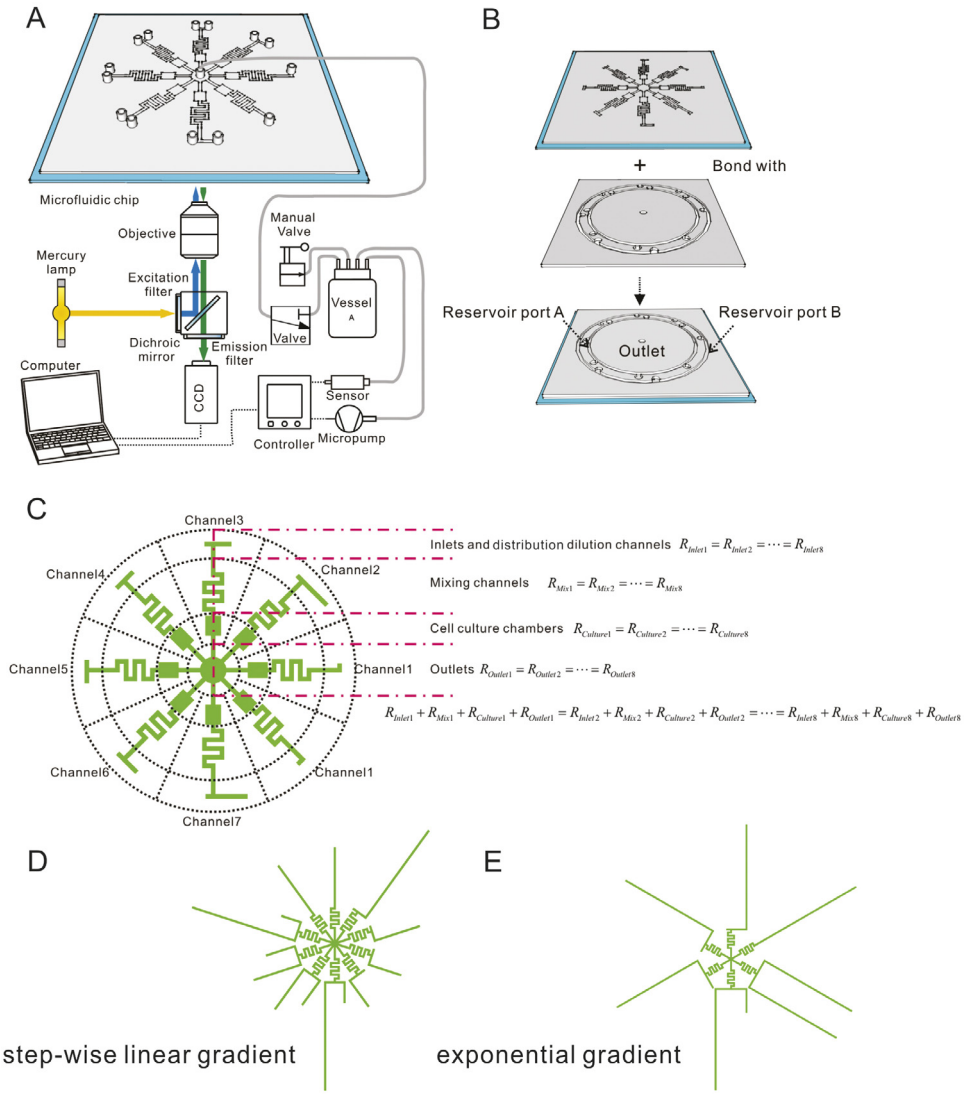

Fig. 1. Chip design and set ups. (A) Schematic of experimental setup for single-step confluent gradient dilution. (B) Schematic an alternative of reservoir A and B. (C) designs of linear gradient dilution device showing four modules: outlets, cell culture chambers, mixing channels and bifurcate dilution channels (D) designs of logarithmic gradient dilution device (E) design of custom gradient dilution device.

incubated (5% CO_2, 90% humidified) at 37 °C in an incubator (Innova-Co 170, New Brunswick Scientific, UK) prior to use. Cells were subcultured at a ratio of 1:3 every three days to maintain cells in the exponential growth phase. Cells were detached from the flask with the treatment of 0.25% (w/v) Trypsin-EDTA solution (Gibco) for 3 min for harvest. Cells were then suspended in the culture media at a concentration of 1×10^5 cells/mL before use.

2.4. Fabrication of microfluidic chip

The microfluidic single-step dilution chips were fabricated according to the rapid prototyping method as previously reported. In brief, SU-8 1070 (Gersteltec Sarl, Switzerland) mold was fabricated on a silicon wafer n type ⟨1 0 0⟩ using standard soft-lithography technique. The PDMS layer, made from a mixture of 10:1 (m/m) PDMS and curing agent (Sylgard 184, Dow Corning, USA), was fabricated by molding the SU-8 structure. Then the PDMS sheet was cut and peeled from the mold. Holes of the inlets and outlet were punched using a hole puncher. The PDMS was irreversibly bonded to a cover glass slide after treatment of oxygen plasma. Reservoir ports were bonded to the punched holes using the epoxy glue (Fig. 1A and B).

2.5. Operation procedures

A custom-built pressure control system was employed to realize automatic pressure control (Fig. 1A). A negative pressure was applied to the outlet via a separate 1 L air container, which was controlled by a micropump (FM2002, Ruiyi, China). To stabilize the pressure, container was monitored by a pressure sensor (PSE541, SMC, Japan) and a sensor controller (PSE200, SMC, Japan). The micropump could be toggled on/off with a resolution of 0.1 kPa. To switch between negative pressure and atmosphere at outlet, a three-way solenoid operated valve (Series 33, MAC, USA) was connected between the outlet and the air container, which was controlled with a home-built software program (LabVIEW TM 7.1).

2.6. Optical imaging system

An inverted fluorescence microscope (IX71, Olympus, Japan) with a CCD camera (Evolve 512, photometrics, USA) were used for

multidrug resistance analysis. Flow visualization experiments were monitored under a 10X objective lens (N.A. 0.3) with a filter cube of U-MWIB2 (460–490 nm band-pass filter, 505 nm diachronic mirror, 510 nm high-pass filter, Olympus, Japan). Cube of U-MWG2 (510–550 nm band-pass filter, 570 nm diachronic mirror, 590 nm high-pass filter, Olympus, Japan) and U-MWIB2 (460-490 nm band-pass filter, 505 nm diachronic mirror, 510 nm high-pass filter, Olympus, Japan) were used for fluorescence co-localization and gradient efflux inhibition assay.

2.7. CFD simulation

Numerical simulations were carried out to investigate the structure of the microfluidic single-step dilution chip using the simulation software Fluent 6.1. The dilution efficiency was validated using a 3D finite volume model. The simulation procedure adopted was similar to the description by Mendels et al. The distribution of the species concentration was obtained by solving the continuity equation, Navier-Stokes equation and diffusion-convection equation. The properties of fluids for the simulation are Newtonian with density 10^3 kg m^{-3}, viscosity 10^{-3} Pa s and diffusion coefficient 4.9×10^{-10} m^2/s (fluorescein in water). For the inlets, one stock solution was the pure water, the other was simulated solute. The concentrations for the two solutions were set as 0 and 1. The criterion for convergence was set for the increment in each variable to fall below 1×10^{-5}.

3. Results and discussion

3.1. Designs of linear, logarithmic and custom dilution

The proposed dilution device was designed based on the hydrodynamic theory (Fig. 1C–E). For the linear dilution design shown in Fig. 1C, the structure of the single-step dilution chip had eight parallel channels, and each channel was divided into four modules: outlet, cell culture chamber, mixing channels and distribution channels. A negative pressure was applied on the outlet module to drive eight parallel flows. Liquids in the reservoirs would firstly flow into the distribution channels, the length of which determined the mixing ratio of two stock solutions. Then, distributed liquids would be fully mixed in the mixing channels. Finally, cells growing in cell culture chambers were stimulated using the diluted liquids for cell-based assay. More importantly, cells in the cultivation chamber won't interfere with the concentration, since the concentration was only determined by the ratio of the length of the distribution channels. The hydrodynamic resistance of outlet, cell culture chamber and mixing channel in parallel channels were the same due to the same structure. For the distribution channels module, there is an inverse relationship between the flow rates of the two solutions and the lengths of the distribution channels, as presented in Eq. (4). In all parallel eight channels, the design of the distribution channel modules was flexible. The lengths of the distribution channels were presented in Table S1. The exponential dilution and piecewise linear dilution were designed based the same principles. The designs of the exponential dilution and stepwise linear dilution were shown in Fig. 1D and E. The lengths of the distribution channels of the exponential dilution and stepwise linear dilution were presented in Tables S2 and S3. Further, the designs were validated using CFD simulation and flow visualization experiments.

3.2. CFD simulation of linear, exponential, and piecewise linear dilution

A numerical study was conducted in this paper to validate the designs of the dilution devices of linear gradient, exponential gradient and piecewise linear gradient (Fig. 2). To demonstrate the dilution ratio of different channels, a dilute solution (water) and a stock solution (100%, 0% equals to water) were used as the materials.

At a flow pressure of 8 kPa, the dilution result of two dilute solutions (water and 100% stock solution) in linear gradient dilution device was shown as Fig. 2A. At the confluent points, the ratios of the widths of two solutions increased as shown, which were resulted from the relative lengths of the distribution channels, i.e., the resistances of the channels. The mixing efficient was also validated shown in Fig. 2A–C. After the clear fluid interface seen at

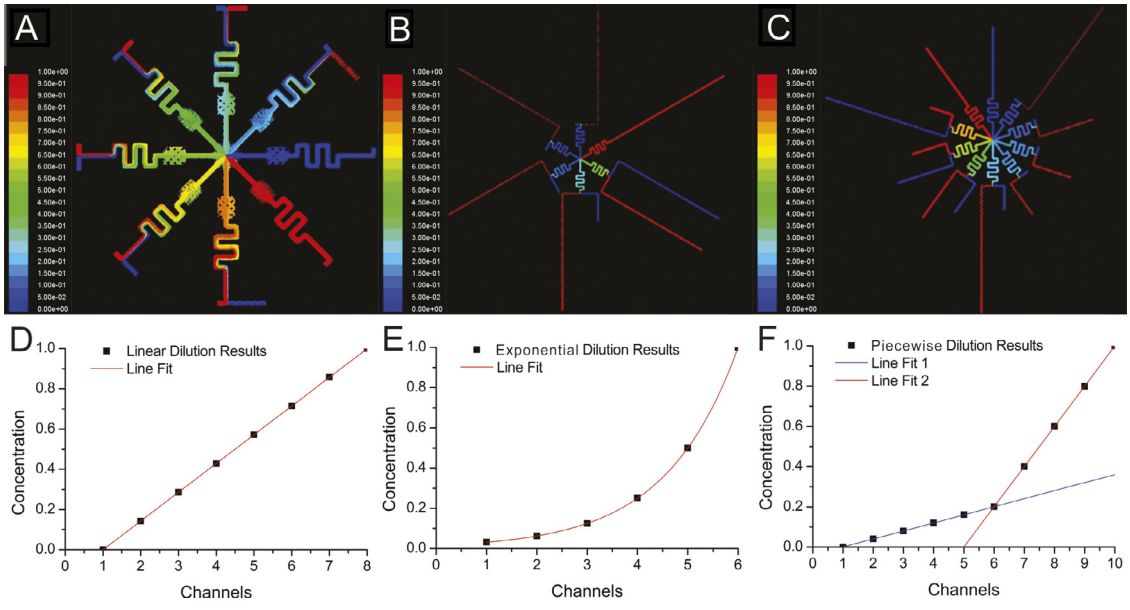

Fig. 2. Results of CFD simulation. (A) Visible numerical study results of linear gradients dilution design. (B) Visible numerical study results of exponential gradients dilution design. (C) Visible numerical study results of piecewise gradients dilution design. (D) Concentrations in each channels of linear gradients dilution design. (E) Concentrations in each channels of exponential gradients dilution design. (F) Concentrations in each channel of piecewise gradients dilution design. Data shown in (D–F) were calculated as the average intensities of species in a cross-section area of the channels.

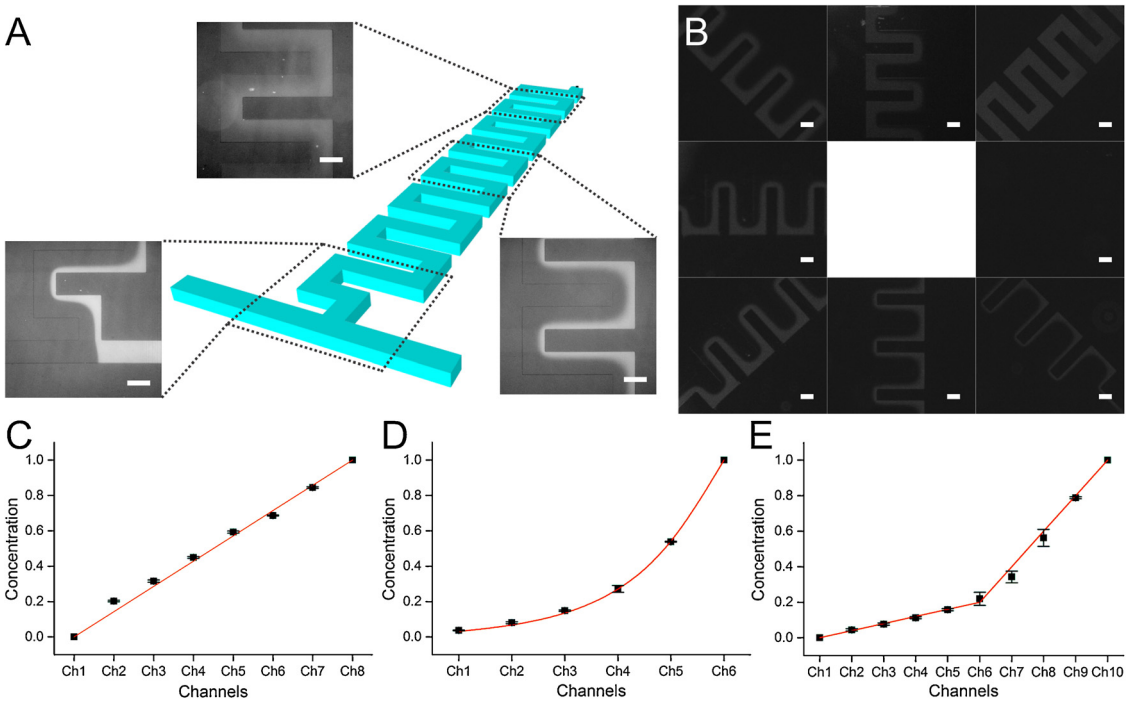

Fig. 3. Results of flow visualization experiments. (A) Details of mixing efficient in long mixing channel. (B) Distribution of two stock solutions in each channel of linear dilution device. (C) Quantitative analysis of linear gradients dilution design. (D) Quantitative analysis of exponential gradients dilution design. (E) Quantitative analysis of piecewise gradients dilution design. Data shown in (C–E) were calculated as the average intensities of species in a cross-section area of the channels. Scale bar, 200 μm.

the confluent points, mixing began to occur and the interface was not so clear. At the end of the eight serpentine mixing channels, the color showed complete mixing achieved here. At the end of the serpentine channels where the mixing was completed, the average intensities in a cross-section area of the channels were calculated to validate the linear dilution. The results were shown in Fig. 3D. The correlation coefficients of linear regression, R^2, for the linear dilution design was higher than 0.999.

The designs of exponential dilution (Fig. 1E) and piecewise linear dilution (Fig. 1D) were also examined using numerical study. The numerical concentration maps were shown in Fig. 2B (exponential dilution) and Fig. 2C (piecewise linear dilution). The average intensities of species in a cross-section area of the channels were also calculated. The concentration profiles were shown in Fig. 2E (exponential dilution) and Fig. 2F (piecewise linear dilution), which were consistent with the theoretical results. To sum up, the results of CFD simulation confirmed that microfluidic chips of the proposed designs could successfully generate linear, exponential and piecewise linear dilution by simply adjusting the length of the distribution microchannels.

3.3. *Flow visualization experiments of linear logarithmic custom dilution*

Flow visualization experiments were performed on chips using fluorescein. Mixed flows of two distribution liquids at the confluent channels were observed (Fig. 3A, Fig. S1 and Supporting information). The diffusion of two distribution liquids was observed in the middle of Serpentine channels. The detection point was set at the ends of the serpentine channels, where two flows were completely mixed. As shown in Fig. 3B, the ratio of the widths of two liquids at the confluent point of the mixing channel changes according to the ratio of the distribution channels length changing (Fig. 3B).

The final concentrations were calculated as a ratio of the final fluorescence intensities and the initial fluorescence intensities (100% stock solution). The concentration profiles (shown in Fig. 3C–E) were consistent with the theoretical and numerical results, confirming the relative lengths of the distribution channels determined the mixing ratio of the two stock solutions. Moreover, varied pressure (8 kPa, 12 kPa and 16 kPa) were applied to the device as the driving force, we get the same concentration profile. That means varied flow rate would result in a same concentration. Unlike the commonly used diffusion-based methods and serial dilution based methods, in which the fluctuation of the flow rate and pressure would dramatically change the profile of the concentration gradient, particularly, at low flow rate with non-negligible pulsation of flow due to the size of the syringes employed and the dyssynchrony between the syringes employed in this experiment. This single-step dilution device is more advantageous since the gradient profile is fixed no matter how the driven pressure or flow rate changes. The chemical concentration in eight channels of the linear dilution chip could be well fitted with linear functions (Fig. 3C). The correlation coefficients of linear regression, R^2, for the linear dilution chip was higher than 0.99. Quantitative analyses of exponential dilution chip and piecewise dilution chip were summarized in Fig. 3D and E. The chemical concentrations were well fitted with exponential (Fig. 3D) and piecewise linear (Fig. 3E) functions (both $R^2 > 0.99$). The error bars means the standard deviation of five parallel experiments using different devices, which confirm that our device have a good repeatability and reproducibility.

Additionally, our device is also easily scaled up by simply adding more parallel microchannels. Since parallel microchannels work independently, making more concentrations will not sacrifice the stabability, repeatability and reproducibility. Here, we further fabricate a device with 64 channels of different concentrations. The design and the device were shown in Fig. S2A and S2C respectively. The lengths of the distribution channels were presented in table S4. The fluorescein solution and the buffer solution were used

as to generate gradient concentrations. The final concentrations generated in individual channels were calculated as a ratio of the final fluorescence intensities and the initial fluorescence intensities (100% stock solution). The results were well fitted with the theoretical profile (shown in Fig. S2B), which confirm that our device can precisely generate a large number of concentrations. Another 64-channel device with parallel concentrations was fabricated to generate eight parallel linear concentrations (Fig. S2D). The concentrations generated in each channels were calculated and fitted with theoretical profile (shown in Fig. S2E). Thus, we demonstrated the proof-of-concept of large scale concentrations generator. However, there are still some limitations of our design. To further improve the throughput and meet the requirement of industrial applications, several possible ways were presented and discussed in the supporting information.

3.4. Analysis of time-dependent drug efflux kinetics

One major drawback of the conventional MDR analysis using fluorescence plate reader and flow cytometry is that it does not provide real time drug transport kinetic information of individual cells. Here, our device is used to record the drug efflux kinetics of single cell. Further, we demonstrated the drug efflux kinetics in a single cell can be inhibited by a common modulator of MDR-associate protein cyclosporin A using our device.

Firstly, drug efflux kinetics was analyzed using a different-single-cell analysis strategy. HepG2 cells were cultured in cell culturing chamber of the chip prior to time-dependent drug efflux experiments. Fluo-3/AM solution of a concentration of 1 μM was loaded into the cell culturing chamber for incubation. After 15 min incubation, Fluo-3/AM was accumulated inside individual cells. Buffer solution was then pumped into the chip to remove the residual extracellular Fluo-3/AM in the medium. An optical detection system consisting of an inverted microscope was employed for simultaneous fluorescence measurement. We tracked the fluorescence intensity of individual HepG2 cells. Then, the procedure was repeated on a second chip. Briefly, cells were treated with 1 μM Fluo-3/AM for 15 min. The drug efflux was then conducted in buffer solution containing a MDR modulator cyclosporin A. The time-dependent fluorescent intensity was measured. The fluorescent curves with and without cyclosporin A were depicted in the diagram shown in Fig. 4A. It was observed that the Fluo-3 efflux was fast at the early stage (0–500 s). Then, the drug efflux rate slowed down and the fluorescence of individual cell did not change significantly. More importantly, less Fluo-3 was retained when the efflux was carried out in the buffer solution comparing to the efflux conducted in cyclosporin A solution. The reason of this observation should be that cyclosporin A could directly bind to MDR-associated protein and inhibite the pump efflux. However, a rare case of more Fluo-3 efflux retained in buffer solution than in cyclosporin A solution was also observed (shown in Fig. 4A). This observation might be resulted from the heterogeneity of individual cells. For instance, cell tested in buffer solution has lower drug efflux ability while cell tested in cyclosporin A solution has a higher drug efflux ability. Practically, not also the cells express MDR-associated protein, only cells obviously exhibit drug efflux were analyzed.

Investigation of drug efflux kinetics was also conducted using a same-single-cell strategy. In this case, 2 cycles of Fluo-3/AM accumulation and efflux steps were demonstrated on the same single cell using the same chip. As shown in Fig. 4B, the two fluorescence curves were obtained from the same single cell. Using the same-single-cell strategy, drug efflux kinetic analysis can be demonstrated regardless of the heterogeneity among cell lines. To sum up, time-dependent drug efflux kinetics can be efficiently analyzed using our device in two different ways.

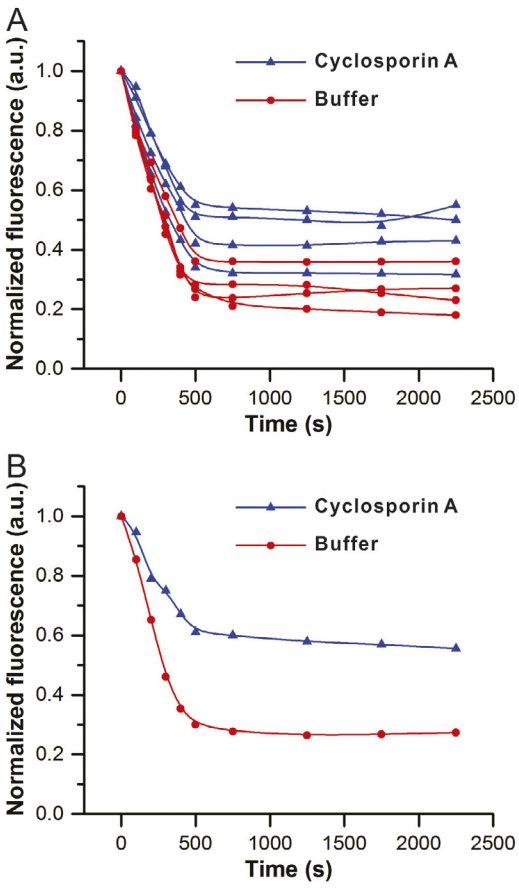

Fig. 4. On-chip analysis of time-dependent drug efflux kinetics. (A) Different-single-cell analysis of time-dependent drug efflux kinetics. Blue curves indicated drug efflux of individual cells conducted in cyclosporine A solution. Red curves indicated drug efflux of individual cells conducted in buffer solution. (B) Same-single-cell analysis of time-dependent drug efflux kinetics. Blue curve indicated drug efflux of individual cell conducted in cyclosporine A solution. Red curve indicated drug efflux of individual cell conducted in buffer solution. (For interpretation of the references to color in this figure legend, the reader is referred to the web version of the article.)

3.5. Polarization of HepG2 and co-localization of MRP2 and fluo-3 secretion

Chemotherapeutics are the most widely used and effective treatment for metastatic tumors. However, multidrug resistance is still a major impediment to successful chemotherapy. Multidrug resistance enables cancer cells to become simultaneously resistant to different drugs. Resistance to natural-product hydrophobic drugs is a general type of multidrug resistance, in which Multidrug resistance associated proteins (such as MRP2) play a dominant role as efflux pumps. Here, human hepatoma HepG2 cells were selected as model cells, which had retained many hepatocyte-specific functions including albumin and bile acid synthesis. HepG2 cells were cultured in chips for several days. Hepatic polarity with phase-lucent bile canaliculus-like structures was formed between adjacent cells. Immunofluorescence assay was used to indicate expression of the conjugate export pump MRP2 in the membrane surrounding the apical vacuoles, which is structurally and functionally analogous to the canalicular membrane in forming microvilli and expressing at least some canalicular proteins. Immunofluorescence staining was carried out as described previously using the following primary antibody dilutions (in PBS): 1:150 for Rabbit-anti-MRP2. TRITC-labeled goat anti-rabbit IgG (1:200 in PBS) was used as the secondary antibody. To further identify the secretion of fluorescent substrate fluo-3 into apical vacuoles, polarized HepG2

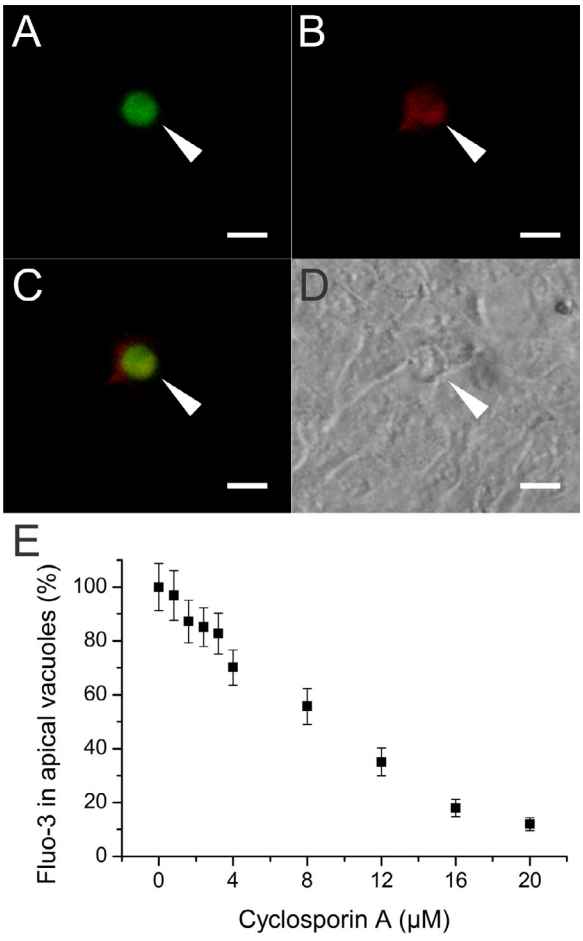

Fig. 5. Single-organelle analysis based on the apical vacuoles of the HepG2 cells. (A) Fluorescent image of apical vacuoles filled with fluo-3. (B) Immunofluorescene staining of apical vacuole using Rabbit-anti-MRP2 and Goat-anti-Rabbit IgG/TRITC. (C) Overlay image of (A and B). (D) Image of apical vacuole in bright field. Scale bar is 10 μm. (E) Quantitative analyzing the percentage of fluo-3 filled apical vacuoles with gradients of cyclosporin A.

cells were loaded in medium with 1 μM fluo-3/AM for 15 min at 37 °C. This time period was proved to be optimal for intracellular formation of the fluorescent substances and their secretion into the apical vacuoles as described previously. It is necessary to rinse cells in medium to ensure viability of the cells. Image of apical vacuoles filled with fluo-3 were taken (Fig. 5A). To verify that the substrate-filled structures were indeed apical vacuoles of HepG2 cells, cells in chip were fixed. And then, immunofluorescence staining was carried out using Rabbit-anti-MRP2 and Goat-anti-Rabbit IgG/TRITC (Fig. 5B). This result demonstrated localization of MRP2 in the apical membrane of HepG2 cells. Immunofluorescence micrographs matching the corresponding micrographs of the fluorescent substrate-filled apical vacuoles were taken to confirm that the fluo-3 filled structure was an apical vacuole (Fig. 5C). Image of apical vacuole in bright field was also taken shown in Fig. 5D. The results revealed that fluo-3 is also a substrate for human MRP2 in multidrug resistance condition.

Our results showed that HepG2 cells were polarized in our microfluidic device and could function well like the native liver tumor cells. Practically, Human MRP2 was expressed and is functionally active in transporting fluorescent amphiphilic anions such as Fluo-3. To sum up, our results confirmed that these polarized HepG2 cells could be used as an efficient chip-based model for multi-drug resistance analysis.

3.6. Inhibition of secretion of fluorescent substrates into vacuoles of HepG2 cells

The cyclosporine A was used as an inhibitor of MRP secretion. The stock solution cyclosporine A preparation (50 mg/ml) contained 33% ethanol, castor oil, and polyoxyethylethanol (650 mg/ml). The blank control solution without cyclosporine A contained Cremophor EL (solvent for cyclosporine A). The stock cyclosporine A solution was diluted to 20 μM before loaded into the reservoir port A. The reservoir port B was loaded with the buffer solution. For analysis of fluo-3 secretion inhibition, HepG2 cells were polarized on microfluidic chip. Cells were incubated in medium with inhibitors of gradient concentration generated by single-step dilution device at 37 °C (0, 0.8, 1.6, 2.4, 3.2, 4, 8, 12, 16, 20 μM). After 2 h incubation, the cells were then rinsed using medium to ensure the removal of extracellular inhibitors that might interfere with the uptake of fluo-3/AM. Thus, the chips were loaded with 1 μM flo-3/AM for 15 min at 37 °C. The chip was washed in cold Ty buffer before observed on a fluorescence microscope. Fluorescent apical vacuoles (fluo-3 filled) were counted in 10 fields with a square size of 678 μm × 678 μm. The numbers of fluorescent apical vacuoles in inhibitor solution of gradient concentration were firstly expressed as percentage of the total number of apical vacuoles. And then, the relative value in each condition was calculated as the ratio to the number of the control group without inhibitor. For each concentration, three independent chips with totally 30 cell cultivation chambers and at least 500 cells were analyzed.

As shown in Fig. 5E, the number of fluo-3 filled fluorescent apical vacuoles decrease as the increasing concentrations of cyclosporine A in the medium. The error bar represents the standard deviation. In the presence of 20 μM cyclosporine A, the number of fluorescent vacuoles was reduced to 12%, compared with the number in the absence of cyclosporine A. The percentage of fluorescent apical vacuoles was 18 ± 3.2% under the treatment of 16 μM, 35.1 ± 5.2% under the treatment of 12 μM, 55.7 ± 6.6% under the treatment of 8 μM, 70.1 ± 6.5% under the treatment of 4 μM, 100 ± 8.72% under the treatment of 0 μM. However, cells were incubated with the inhibitors, which might cause a decrease in cell viability and in density of the apical vacuoles. The ratios of the number of apical vacuoles to the number of cells in the absence and presence of different inhibitors were determined. The ratios were 0.26 ± 0.03 (control, no inhibitor), 0.25 ± 0.04 (12 μM cyclosporine A), and 0.22 ± 0.07 (20 μM cyclosporine A), respectively, indicating that cyclosporine A had no significant effect on the density of apical vacuoles within 2 h incubation.

With apical vacuoles formed by the polarized HepG2 cells, multidrug-resistance analysis was performed in a high-throughput way with single organelle resolution. Hundreds of cells were analyzed at the same time, which provide a higher throughput than other microfluidic-based multi-drug resistance analysis device.

3.7. High-throughput drug screening of chemo-sensitizing compounds

Inhibitor or modulator of MDR-associate protein, such as cyclosporin A, can reverse the multidrug resistance condition of cancer cells by inhibiting the pump efflux to result in an increased intracellular accumulation of the cytotoxic drug, which can be used as chemo-sensitizing compounds to enhance the clinical effect of chemotherapy. Screening of such chemo-sensitizing compounds with minimized adverse effect can extend their clinical use and benefit cancer treatment. Here, our device was further demonstrated as a high-throughput drug screening platform for investigation of both the chemo-sensitizing effect and the cytotoxity of MDR modulators.

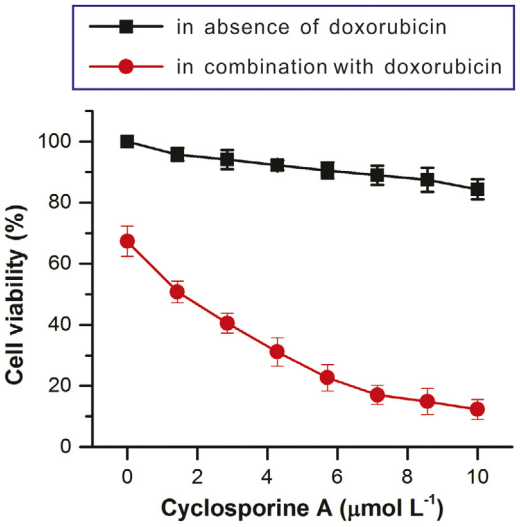

Fig. 6. Quantitative analyzing the chemo-sensitizing effect and the cytotoxity of the cyclosporine A.

Practically, Cyclosporine A was tested for chemo-sensitizing effects on doxorubicin sensitivity. Doxorubicin was chosen as a model of chemotherapy drug. HepG2 cells were cultured in cell culture chambers of the microfluidic chip. Cyclosporine A solution was diluted in 0.2 μg mL^{-1} doxorubicin stock solution to a final concentration of 10 μmol L^{-1}, which was loaded into reservoir A. Doxorubicin stock solution without cyclosporine A was loaded into reservoir B. Linear gradient concentrations of Cyclosporine A combined with doxorubicin of a constant concentration were generated in the sing-step dilution chip and delivered to HepG2 cells for stimulation (using chip design shown in Fig. 1C). After 24 h incubation, Live/Dead assay was carried out to validate the cell viability. The possible cytotoxicity of cyclosporine A in the absence of doxorubicin was also tested in our device in the same way by using doxorubicin-free stock solution. The results were summarized in Fig. 6, which indicated that the simultaneous administration of cyclosporine A and doxorubicin enhanced the cytotoxicity of doxorubicin in a dose-dependent manner. This result revealed that chemotherapy in combination with inhibitors or modulators of MDR-associated protein is a promising strategy for cancer treatment. Conclusively, both the chemo-sensitizing effect and the cytotoxicity of drugs can be studied with our device. The proposed single-step dilution device could be further used as a high throughput tool for drug screening of chemo-sensitizing compounds, which can be used to reverse MDR and further enhance the effect of chemotherapy.

4. Conclusions

A single-step microfluidic dilution system was developed in this paper. The dilution gradient profile could be customized for different use. Once the device is fabricated, the gradient profile is fixed. This single-step microfluidic dilution device was easy-to-operate and much more stable than the diffusion devices and serial dilution devices. The gradient was determined by the lengths of distribution microchannels rather than the complex pattern in conventionally serial dilution approaches, which remarkably reduced the redundancy of microfluidic architecture and made our design easily scalable. As much as 64 different concentrations were generated in single device. This versatile device was further used for multidrug resistance analysis in three different ways. Firstly, time-dependent drug efflux kinetics was measured on the chip using both the different-single-cell analysis strategy and the same-single-cell analysis strategy. Secondly, HepG2 was polarized and the apical vacuoles were formed on this microfluidic device. Immunofluorescence assay was carried out to detect the MRP2 (a kind of multidrug resistance associated protein) expressed on the apical vacuoles. Co-localization was further performed to visualize the substrate pumped into the apical vacuoles with fluo-3. Inhibition of fluorescent substrates secretion into apical vacuoles was also studied with gradient cyclosporine A generated using single-step dilution chip. In this case, MDR was analyzed at single organelles level with high-throughput. Finally, our device was further used as a high-throughput drug screening system for investigation of both the chemo-sensitizing effect and the cytotoxicity of MDR modulators, which can be used as chemo-sensitizing compounds to reverse MDR and further enhance the effect of chemotherapy. In comparison with other two chip-based multidrug resistance analysis method, our device provides a much higher throughput. Practically, Li's group developed a multi-drug resistance analysis system with the ability to record the dynamic information of drug efflux and reveal heterogeneity of MDR in single cell level. However, they can only analyze one cell for one time. And for each cells, it takes more than half an hour to obtain the results. Yoshimi Matsumoto et al. have developed another microchannels-based multidrug efflux analysis device, which might have higher throughput.[37,38] However, they only test populations of bacteria, and fails to obtain the single cell information and efflux dynamic kinetic information. Here, our method has made some improvements. Multiple information, including drug efflux kinetics, drug cytotoxicity and chemo-sensitizing effect, could be tested at single-cell or even single-organelle resolution with advantages of high-throughput, flexibility, stability and low sample consumption, thus further paved a new avenue for high-throughput drug screening for chemo-sensitizing agents.

Acknowledgements

We gratefully acknowledge the financial supports from National Natural Science Foundation of China (21475049, 31471257 and 21275060) and National Basic Research Program of China (2011CB910403).

Appendix A. Supplementary data

Supplementary data associated with this article can be found, in the online version, at http://dx.doi.org/10.1016/j.snb.2015.11.097.

References

[1] M.M. Gottesman, T. Fojo, S.E. Bates, Multidrug resistance in cancer: role of ATP-dependent transporters, Nat. Rev. Cancer 2 (2002) 48–58.
[2] L.J.V. Piddock, Multidrug-resistance efflux pumps – not just for resistance, Nat. Rev. Microbiol. 4 (2006) 629–636.
[3] C. Holohan, S. Van Schaeybroeck, D.B. Longley, P.G. Johnston, Cancer drug resistance: an evolving paradigm, Nat. Rev. Cancer 13 (2013) 714–726.
[4] C.F. Higgins, Multiple molecular mechanisms for multidrug resistance transporters, Nature 446 (2007) 749–757.
[5] M. Dean, T. Fojo, S. Bates, Tumour stem cells and drug resistance, Nat. Rev. Cancer 5 (2005) 275–284.
[6] M.S. Jin, M.L. Oldham, Q.J. Zhang, J. Chen, Crystal structure of the multidrug transporter P-glycoprotein from *Caenorhabditis elegans*, Nature 490 (2012) 566.
[7] S. Murakami, R. Nakashima, E. Yamashita, T. Matsumoto, A. Yamaguchi, Crystal structures of a multidrug transporter reveal a functionally rotating mechanism, Nature 443 (2006) 173–179.
[8] W. Loscher, H. Potschka, Drug resistance in brain diseases and the role of drug efflux transporters, Nat. Rev. Neurosci. 6 (2005) 591–602.
[9] E. Marthinet, G. Divita, J. Bernaud, D. Rigal, L.G. Baggetto, Modulation of the typical multidrug resistance phenotype by targeting the MED-1 region of human MDR1 promoter, Gene Ther. 7 (2000) 1224–1233.
[10] A. Persidis, Cancer multidrug resistance, Nat. Biotechnol. 17 (1999) 94–95.
[11] A.T. Nies, D. Keppler, The apical conjugate efflux pump ABCC2 (MRP2), Pflug. Arch. Eur. J. Phys. 453 (2007) 643–659.

[12] K.M. Tainton, M.J. Smyth, J.T. Jackson, J.E. Tanner, L. Cerruti, S.M. Jane, et al., Mutational analysis of P-glycoprotein: suppression of caspase activation in the absence of ATP-dependent drug efflux, Cell Death Differ. 11 (2004) 1028–1037.
[13] S.I. Akiyama, M.M. Cornwell, M. Kuwano, I. Pastan, M.M. Gottesman, Most drugs that reverse multidrug resistance also inhibit photoaffinity-labeling of P-glycoprotein by a vinblastine analog, Mol. Pharmacol. 33 (1988) 144–147.
[14] A. Pawarode, S. Shukla, H. Minderman, S.M. Fricke, E.M. Pinder, K.L. O'Loughlin, et al., Differential effects of the immunosuppressive agents cyclosporin A, tacrolimus and sirolimus on drug transport by multidrug resistance proteins, Cancer Chemoth. Pharm. 60 (2007) 179–188.
[15] E.J. Wang, C.N. Casciano, R.P. Clement, W.W. Johnson, HMG-CoA reductase inhibitors (statins) characterized as direct inhibitors of P-glycoprotein, Pharm. Res. Dordr. 18 (2001) 800–806.
[16] S. Warmann, G. Gohring, B. Teichmann, H. Geerlings, J. Fuchs, MDRI modulators improve the chemotherapy response of human hepatoblastoma to doxorubicin in vitro, J. Pediatr. Surg. 37 (2002) 1579–1584.
[17] T. Efferth, M. Davey, A. Olbrich, G. Rucker, E. Gebhart, R. Davey, Activity of drugs from traditional Chinese medicine toward sensitive and MDR1- or MRP1-overexpressing multidrug-resistant human CCRF-CEM leukemia cells, Blood Cell Mol. Dis. 28 (2002) 160–168.
[18] J. Ford, P.G. Hoggard, A. Owen, S.H. Khoo, D.J. Back, A simplified approach to determining P-glycoprotein expression in peripheral blood mononuclear cell subsets, J. Immunol. Methods 274 (2003) 129–137.
[19] B.C. Medeiros, H.J. Landau, M. Morrow, R.O. Lockerbie, T. Pitts, S.G. Eckhardt, The farnesyl transferase inhibitor, tipifarnib, is a potent inhibitor of the MDR1 gene product, P-glycoprotein, and demonstrates significant cytotoxic synergism against human leukemia cell lines, Leukemia 21 (2007) 739–746.
[20] J. Wu, Q.S. Chen, W. Liu, J.M. Lin, A simple and versatile microfluidic cell density gradient generator for quantum dot cytotoxicity assay, Lab Chip 13 (2013) 1948–1954.
[21] Y. Li, X. Feng, Y. Wang, W. Du, P. Chen, C. Liu, et al., Assembly of multiple cell gradients directed by three-dimensional microfluidic channels, Lab Chip 15 (2015) 3203–3210.
[22] Y.W. Li, X.J. Feng, W. Du, Y. Li, B.F. Liu, Ultrahigh-throughput approach for analyzing single-cell genomic damage with an agarose-based microfluidic comet array, Anal. Chem. 85 (2013) 4066–4073.
[23] Y.W. Li, X.H. Yan, X.J. Feng, J. Wang, W. Du, Y.C. Wang, et al., Agarose-based microfluidic device for point-of-care concentration and detection of pathogen, Anal. Chem. 86 (2014) 10653–10659.
[24] E.K. Sackmann, A.L. Fulton, D.J. Beebe, The present and future role of microfluidics in biomedical research, Nature 507 (2014) 181–189.
[25] X.J. Li, Y.C. Chen, P.C.H. Li, A simple and fast microfluidic approach of same-single-cell analysis (SASCA) for the study of multidrug resistance modulation in cancer cells, Lab Chip 11 (2011) 1378–1384.
[26] X.J. Li, V. Ling, P.C.H. Li, Same-single-cell analysis for the study of drug efflux modulation of multidrug resistant cells using a microfluidic chip, Anal. Chem. 80 (2008) 4095–4102.
[27] M.A. Holden, S. Kumar, A. Beskok, P.S. Cremer, Microfluidic diffusion diluter: bulging of PDMS microchannels under pressure-driven flow, J. Micromech. Microeng. 13 (2003) 412–418.
[28] M.A. Holden, S. Kumar, E.T. Castellana, A. Beskok, P.S. Cremer, Generating fixed concentration arrays in a microfluidic device, Sens. Actuators B: Chem. 92 (2003) 199–207.
[29] K. Campbell, A. Groisman, Generation of complex concentration profiles in microchannels in a logarithmically small number of steps, Lab Chip 7 (2007) 264–272.
[30] S.K.W. Dertinger, D.T. Chiu, N.L. Jeon, G.M. Whitesides, Generation of gradients having complex shapes using microfluidic networks, Anal. Chem. 73 (2001) 1240–1246.
[31] C. Kim, K. Lee, J.H. Kim, K.S. Shin, K.J. Lee, T.S. Kim, et al., A serial dilution microfluidic device using a ladder network generating logarithmic or linear concentrations, Lab Chip 8 (2008) 473–479.
[32] K.W. Oh, K. Lee, B. Ahn, E.P. Furlani, Design of pressure-driven microfluidic networks using electric circuit analogy, Lab Chip 12 (2012) 515–545.
[33] M. Yamada, T. Hirano, M. Yasuda, M. Seki, A microfluidic flow distributor generating stepwise concentrations for high-throughput biochemical processing, Lab Chip 6 (2006) 179–184.
[34] T. Cantz, A.T. Nies, M. Brom, A.F. Hofmann, D. Keppler, MRP2, a human conjugate export pump, is present and transports fluo 3 into apical vacuoles of Hep G2 cells, Am. J. Physiol. Gastrointest Liver Physiol. 278 (2000) G522–G531.
[35] J. Konig, A.T. Nies, Y.H. Cui, I. Leier, D. Keppler, Conjugate export pumps of the multidrug resistance protein (MRP) family: localization, substrate specificity, and MRP2-mediated drug resistance, BBA: Biomembranes 1461 (1999) 377–394.
[36] M. Qadir, K.L. O'Loughlin, S.M. Fricke, N.A. Williamson, W.R. Greco, H. Minderman, et al., Cyclosporin A is a broad-spectrum multidrug. resistance modulator, Clin. Cancer Res. 11 (2005) 2320–2326.
[37] R. Iino, K. Nishino, H. Noji, A. Yamaguchi, Y. Matsumoto, A microfluidic device for simple and rapid evaluation of multidrug efflux pump inhibitors, Front. Microbiol. 3 (2012) 40.
[38] Y. Matsumoto, K. Hayama, S. Sakakihara, K. Nishino, H. Noji, R. Iino, et al., Evaluation of multidrug efflux pump inhibitors by a new method using microfluidic channels, PLoS ONE 6 (2011) e18547.

Biographies

Yiwei Li is a Ph.D. candidate in HUST, China. His research interest focuses on microfluidic-based methods for biological applications and bioengineering.

Dongjuan Chen is a Ph.D. candidate in HUST, China. Her research interest focuses on microseparation and biosensors.

Yifang Zhang is a student pursuing her Master degree in HUST, China. Her research interest focuses on biosensors and mass spectrometry-based glycomics.

Chao Liu is a Ph.D. candidate in HUST, China. His research interest focuses on biosensors and microfluidic-based mixing devices.

Peng Chen is a Ph.D. candidate in HUST, China. His research interest focuses on microfluidic-based cell analysis.

Yachao Wang is a Ph.D. candidate in HUST, China. His research interest focuses on microfluidic-based methods for biological applications and bioengineering.

Xiaojun Feng received his Ph.D. degree in biology from the University at Albany, State University of New York in 2006. Thereafter, he moved to HUST, China, continuing his postdoctoral research in the College of Life Science & Technology. He is currently an Associate Professor at HUST. His research interest includes BioMEMS, microfluidics, point-of-care testing devices and mass spectrometry-based proteomics.

Wei Du received his Ph.D. degree in biology from Wuhan University, China. He is currently an Associate Professor at HUST. His research interest focuses on optical imaging of C. elegans.

Bi-Feng Liu received his Ph.D. degree in analytical chemistry from Wuhan University (China) in 1999 and continued his postdoctoral research in the College of Life Science. From 2001, he moved to Japan and worked in Prof. Terabe's group (Japan) as a JSPS Postdoctoral Fellow. He joined HUST as a Professor in 2003. He is now serving as deputy Dean of the College of Life Science & Technology. His research focuses on systems biology-oriented analytical science in the areas of mass spectrometry coupled micro-separation, microfluidics and molecular imaging.